*Int. J. Electrochem. Sci.*, 15 **(2020)** 3563 – 3577, doi: 10.20964/2020.04.19

**International Journal of**
**ELECTROCHEMICAL**
**SCIENCE**
www.electrochemsci.org

# Hierarchical Porous NiS@NiO Nanoarrays in Situ Grown on Nickel Foam as Superior Electrocatalyst for Water Splitting

*Xiao-Yang Wang, Xiao-Peng Han*, Yu He, Wen-Bin Hu and Yi-Da Deng**

School of Materials Science and Engineering, Tianjin Key Laboratory of Composite and Functional Materials, Tianjin University, Tianjin 300350, China.
*E-mail: xphan@tju.edu.cn; yida.deng@tju.edu.cn.

*Received:* 18 November 2019 / *Accepted:* 8 January 2020 / *Published:* 10 March 2020

---

The development of economic and efficient bifunctional water-sptting catalysts in case of the oxygen evolution reaction (OER) and hydrogen evolution reaction (HER) is of considerable practical significance. Herein, a hierarchical porous NiS@NiO nanoarray with a large surface area was prepared in situ on nickel (Ni) foam as a water-splitting catalyst via a simple hydrothermal method. The core–shell NiS@NiO/NF hybrid exhibits an excellent bifunctional performance with low overpotentials of 150 and 319 mV to achieve an HER current density of 10 mA cm$^{-2}$ and a large OER current density of 100 mA cm$^{-2}$, respectively, in the 1.0 M KOH solution because of its high specific surface area and the interface between the two phases. Furthermore, NiS@NiO/NF exhibits a cell voltage of 1.54 V for overall water splitting and extremely high stability for more than 50 h at 10 mA cm$^{-2}$. This study will help to design and develop high-performance hybrid nanomaterials via interfacial engineering for obtaining clean energy conversion technologies.

---

**Keywords:** Nanocomposite; Heterointerface; Electrocatalysis; HER/OER; Water splitting.

## 1. INTRODUCTION

The current energy deterioration and environmental problems have motivated researchers to seek new fossil fuel alternatives [1-3]. Hydrogen has been considered to be a potential efficient, renewable and environment-friendly clean energy source [4-7] because of its advantages such as abundant reserves, no carbon emissions and sustainablility. Among various hydrogen production methods, the electrolysis of water is considered to be one of the most promising approaches because of its simple operation and high conversion [8-10].

The electrolysis of water can be categorised into two parts, the oxygen evolution reaction (OER), where the oxygen element occurring at anode loses electrons to generate oxygen, and the hydrogen evolution reaction (HER), where the hydrogen element occurring at cathode gains electrons to generate hydrogen. However, a high overpotential considerably higher than the theoretical value is necessary to drive OER and HER because of their intrinsically sluggish catalytic kinetics [11-14]. Therefore, a highly efficient bifunctional electrocatalyst has to be developed for both OER and HER. Currently, noble metal oxides, including $RuO_2$, $IrO_2$ and their alloys, exhibit state-of-the-art OER performance [15,16] and Pt-based catalysts serve as the HER benchmark [17,18]. They exhibit limitations, including scarcity of reserves, high price, low stability and single catalytic function; therefore, these noble metal-based catalysts cannot be applied on a large scale in industrial production. Hence, earth-abundant electrocatalysts exhibiting remarkable bifunctional activity as well as stability is urgently required for overall water splitting.

Recently, transition metals (e.g. Co, Fe, Ni and Mo) and their compounds have been extensively used to study the electrochemical overall water-splitting catalysts [19-26]. Cobalt-based catalysts are proved to exhibit a high electrochemical catalytic performance as well as strong corrosion resistance and stability in a concentrated alkaline environment [27-30]. In particular, cobalt oxides have been considerably investigated because of their simple preparation. However, their inherent poor conductivity and low HER performance limit their practical application. To address the aforementioned problems, catalysts are usually modified by increasing the active area, optimising the intrinsic activity, enhancing the conductivity, etc. The introduction of heterogeneous interface is a good methodology to improve the conductivity of the catalyst because the electrons tend to be delocalised; further, the delocalised electrons would decrease the adsorption energy of the intermediate to enhance the intrinsic activity. Recently, noble metal doping has been considered to be the main method for introducing a heterogeneous interface. However, precious metals are expensive and cannot be utilised on a large scale; therefore, the transition metal sulfide that exhibits similar properties to those of the precious metal issued as the substitute of precious metal to introduce heterogeneous interface[17].

Herein, a three-dimensional (3D) hierarchical porous microsheet, which comprises NiS nanoflakes supported on the NiO substrate to form a core–shell microstructure array coated on the Ni foam (NF, designated as NiS@NiO/NF), was synthesised via a simple one-step hydrothermal sulfuration method for application to overall water splitting in alkaline medium for the first time. This core–shell structure enhances the contact area of the electrolyte using a catalyst and introduces abundant coupled interfaces between NiS and NiO, providing a large number of active sites that exhibit high reactivity for the catalytic reactions. Additionally, the binder-free catalyst that is grown in situ on nickel foam exhibits fast electron transfer rates and long-term stability. The electrochemical results denote that the NiS@NiO/NF electrode exhibits superior catalytic performance with low overpotentials of 150 mV for HER to achieve a current density of 10 mA $cm^{-2}$ and 319 mV for OER to achieve a high current density of 100 mA $cm^{-2}$ in the 1.0 M KOH solution. The NiS@NiO/NF electrode delivers a low cell voltage of 1.54 V at 10 mA $cm^{-2}$ for water electrolysis. These results indicate that the unique hierarchical structure can provide sufficient contact area and that the introduced heterointerface between NiS and NiO can afford highly reactive sites, resulting in the remarkable bifunctional electrochemical performance of overall water splitting.

## 2. EXPERIMENTAL SECTION

### *2.1. Material preparation*

Nickel nitrate 6-hydrate ($Ni(NO_3)_2·6H_2O$, 99.99%), sodium sulfide nonahydrate ($Na_2S·9H_2O$, 99.0%) and ruthenium (IV) oxide ($RuO_2$) were purchased from Adamas Reagent Co. Ltd. Urea ($CO(NH_2)_2$, 99.0%) was purchased from Sinopharm Chemical Reagent Co. Ltd. Ammonium fluoride ($NH_4F$, 96.0%) was purchased from Tianjin Fengchuan Chemical Reagent Technology Co. Ltd. Ethanol ($C_2H_5OH$, 99.7%) and isopropyl alcohol ($(CH_3)_2CHOH$, 99.8%) were purchased from Tianjin Kemiou Chemical Reagent Co. Ltd. Nafion perfluorinated resin solution (5 wt.% in a mixture of lower aliphatic alcohols and water, containing 45% water) was prepared by Sigma Aldrich Co. Ltd. Pt/C (20 wt.%) was purchased from Shanghai Hesen Electric Co. Ltd. Acetone ($CH_3COCH_3$, 99.5%), hydrochloric acid (HCl, 36%) and deionised (DI) water were purchased from Milli-Q. All the aforementioned reagents were of analytical grade and were used without any further purification. The Ni foams (2 cm × 3 cm) were successively pre-washed using acetone, hydrochloric acid (diluted to 6%), DI water and ethanol thrice and were stored in ethanol before use.

### *2.2. Preparation of the $NiCO_3·2Ni(OH)_2·4H_2O$/NF precursor*

First, 0.6 g (1 mmol) of urea, 0.148 g (4 mmol) of $NH_4F$ and 0.58 g (2 mmol) of $Ni(NO_3)_2·6H_2O$ were completely dissolved in 40 mL of DI water via ultrasonic shaking. Subsequently, the mixture was transferred into a 50-mL Teflon-lined stainless steel autoclave. A piece of pretreated Ni foam (2 cm × 3 cm) was placed in the solution and thoroughly mixed via ultrasonic shaking for 10 min to ensure that the nickel foam was in complete contact with the solution. Then, the stainless steel autoclave was placed in an electric oven maintained at 90 °C for 10 h for ageing. As the reactor was cooled to the room temperature, a series of uniform nanosheet $NiCO_3$ $2Ni(OH)_2$ $4H_2O$/NF precursor was grown on the Ni foam, cleaned using DI water and ethanol thrice and finally dried at 60 °C in an electric oven.

### *2.3. Preparation of NiO/NF*

$NiCO_3·2Ni(OH)_2·4H_2O$/NF was added to a muffle furnace and annealed at 300 °C in air for 2 h to prepare NiO/NF.

### *2.4. Preparation of NiS@NiO/NF*

Different quantities of $Na_2S·9H_2O$ (0.2, 0.4, 0.6, 1.0 and 1.2 g) were completely dissolved in 40 mL of DI water via ultrasonic shaking. Subsequently, the solutions were transferred into 50-mL Teflon-lined stainless steel autoclaves along with the dried NiO/NF, and the autoclaves were heated to 120 °C for 10 h. After the reactor was cooled to room temperature, it was rinsed and dried, and samples exhibiting four different sulfurisation degrees with an average loading capacity of 1 mg $cm^{-2}$ were obtained.

### *2.5. Preparation of NiS/NF*

$Na_2S\cdot9H_2O$ (2.0 g) was completely dissolved in 40 mL of DI water via ultrasonic shaking. Subsequently, the solution was transferred into 50-mL Teflon-lined stainless steel autoclaves along with the dried NiO/NF, and the autoclaves were heated to 120 °C for 14 h. After the reactor was cooled to room temperature, NiS/NF was obtained by rinsing with DI water thrice.

### *2.6. Material characterisation*

The phases of the samples were characterised using X-ray diffraction (XRD) (Rigaku D/Max 2500 V/PC), equipped with a Cu Kα source at 40 kV and 200 mA scanning from 10° to 80° at a rate of 6° $min^{-1}$. Further, the micromorphology of the samples was determined using a scanning electron microscope (SEM) (Hitachi S-4800, 15 kV), equipped with an energy-dispersive spectrometer (EDAX Genesis XM2), and a transmission electron microscope (TEM) (JEOL JEM-2100F) operated at 200 kV.

### *2.7. Electrochemical measurements*

The electrochemical catalytic activity (HER and OER) measurements were performed in a standard three-electrode system controlled on a CHI760e electrochemical workstation in a 1.0 M KOH solution at room temperature. A platinum plate exhibiting dimensions of 1 cm × 1 cm was used as the counter electrode, whereas the mercuric oxide electrode (MOE) served as the reference electrode. The prepared electrode materials, which were cut into pieces of 1 cm × 1 cm, were considered to be the working electrode. The contrast electrode samples of Pt/C/NF and $RuO_2$/NF were prepared based on the following steps. First, 3 mg of Pt/C (20 wt.%) or $RuO_2$ was dispersed in 970 μL of isopropyl alcohol. Second, 30 μL of 5 wt.% Nafion were added into the solution as the binder; subsequently, the solution was sonicated for at least 30 min for preparing the catalyst ink. Finally, 350 μL of the catalyst ink (with a loading capacity of 2 mg $cm^{-2}$) was dropped on the Ni foam with dimensions of 1 cm × 1 cm. The MOE reference electrode was adjusted against the reversible hydrogen electrode (RHE) using the following equation: $E_{(RHE)} = E_{(MOE)} + 0.059 \times pH + 0.098$ V. The linear sweep voltammetry (LSV) curves were measured using a scan rate of 5 mV $s^{-1}$, and multi-cyclic voltammetry (CV) cycling was conducted from 0 to 0.9 V vs. MOE for the OER and from −0.7 to −1.5 V vs. MOE for the HER at a scanning rate of 50 mV $s^{-1}$. The geometric double layer capacitances ($C_{dl}$) were determined based on the CV curves at different scanning rates (5, 10, 25, 50 and 100 mV $s^{-1}$) in the potential range from −0.05 to 0.05 V vs. MOE. The electrochemical impedance spectroscopy (EIS) measurements were conducted at 0.7 V vs. MOE for the OER and −1.35 V vs. MOE for the HER from $10^5$ to 0.1 Hz with an AC potential amplitude of 5 mV. The overall water-splitting catalytic performance of the materials was measured using a two-electrode system, which was controlled from the CHI760e electrochemical workstation, in a 1.0 M KOH solution maintained at room temperature. Two identical electrode materials that we have prepared were used as anode and cathode and served as the catalysts to OER and HER; in case of the contrast electrode samples, $RuO_2$/NF was used for the OER on the anode, whereas Pt/NF was used for the HER on the cathode to obtain an electrolytic water system. CV and LSV measurements were performed at scan rates of 50 and 5 mV s$^{-1}$, respectively.

## 3. RESULTS AND DISCUSSION

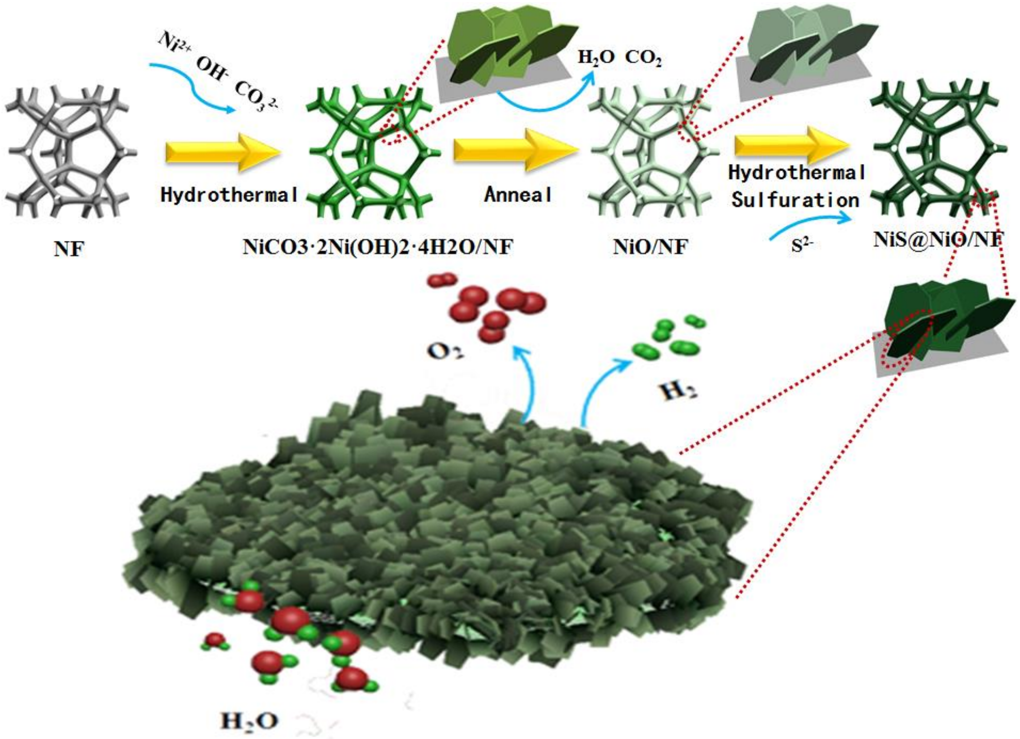

**Figure 1.** Schematic of the preparation of the NiS@NiO/NF hybrid porous electrode.

The schematic of the preparation of NiS@NiO/NF is illustrated in **Fig. 1**. The NiS nanoflakes that were supported on NiO having a high surface area were obtained through various processes, including hydrothermal, oxidation and ion exchange growth sulfurisation. $NiCO_3 \cdot 2Ni(OH)_2 \cdot 4H_2O$/NF was initially deposited on the Ni foam via the hydrothermal method and was subsequently annealed in the air at 300 °C for 2 h to form the NiO/NF precursor. This can be achieved by decomposing the released $H_2O$ and $CO_2$. Subsequently, the sulfur element in the solution combined with the dispersed nickel ions and formed NiS nanoflakes, which assembled on the NiO matrix via a simple and stable one-step hydrothermal sulfurisation process to form the NiS@NiO/NF sample. A large number of nanofilms not only provide more interface but also enhance the specific surface area of the catalyst. Further, four samples with different sulfide content were synthesised and their electrochemistry performances were measured to determine the optimum sulfur ratio. The corresponding SEM images of the samples with different sulfide content are presented in Fig. S1, and the optimal sample was designated as NiS@NiO/NF.

The phases and morphological characterisation of the prepared samples are presented in **Fig. 2**. The NiS@NiO/NF phases were revealed via the XRD patterns (**Fig. 2a**). In addition to the clear nickel peaks observed when 2-theta = 44.5°, 51.8° and 76.4°, diffraction peaks that corresponded to NiS

(JCPDS 02-1280) and NiO (JCPDS 44-1159) could be observed, indicating the successful synthesis of the NiS and NiO compound [31,40,44]. **Fig. 2b** presents the nanosheet array of the NiO grown on the Ni foam, which exhibits a smooth surface.

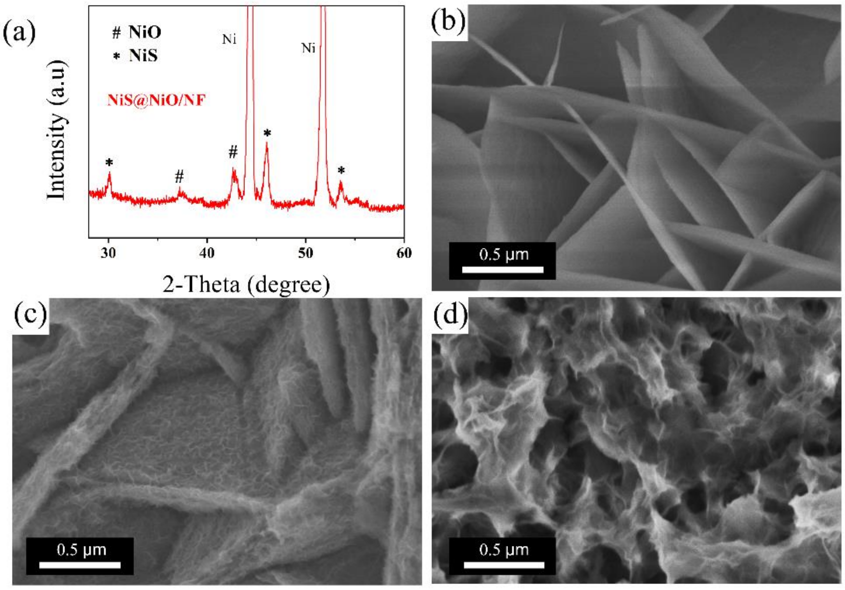

**Figure 2.** (a) XRD pattern of NiS@NiO/NF and SEM images of (b) NiO/NF, (c) NiS@NiO/NF and (d) NiS/NF.

The NiS@NiO/NF, as can be observed in **Fig. 2c**, was obtained via the sulfuration of NiO/NF. The surface of the NiO nanosheets was corroded by $S^{2-}$ and resulted in the in situ formation of a large number of NiS nanoflakes, which constituted a 3D porous structure. Because of the anion exchange growth achieved via a mild sulfurisation process, the sheet-like structure as a bracket was preserved to provide considerable amount of growth areas for obtaining a large number of NiS nanoflakes. This hierarchical structure exhibits an extremely high specific surface area and a heterogeneous interface to provide a large number of electrochemically active sites. **Fig. 2d** denotes the non-bracketed NiS flakes grown on the Ni foam. It is evident that NiS@NiO/NF exhibits a larger surface area than NiO/NF and NiS/NF due to a suitable vulcanization, this greatly facilitates the catalytic reaction.

The morphological structure of NiS@NiO/NF was characterised via a TEM to present the observations obtained at various magnifications. **Fig. 3a** denotes the complete morphology of the NiS@NiO nanosheet with a diameter of approximately 400 nm, which was wrapped by plenty of small NiS nanoflakes.

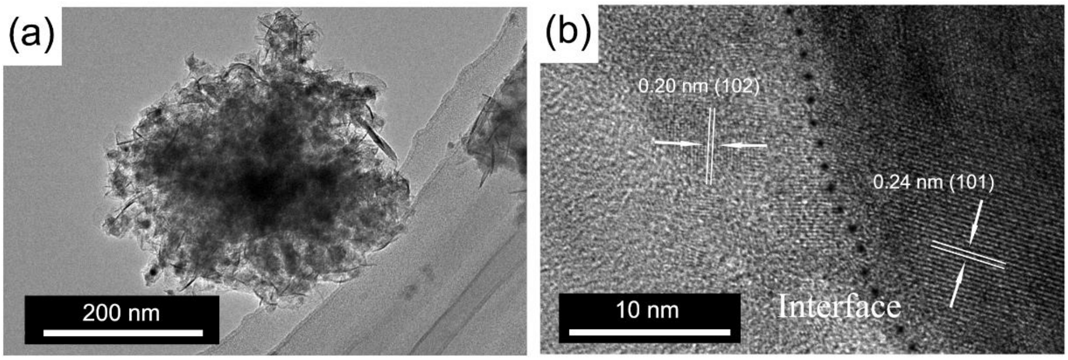

**Figure 3.** (a) Low-resolution and (b) high-resolution transmission electron microscope images of NiS@NiO/NF.

Furthermore, the layered structure, rich porous structure and exposed heterogeneous interface can be observed.

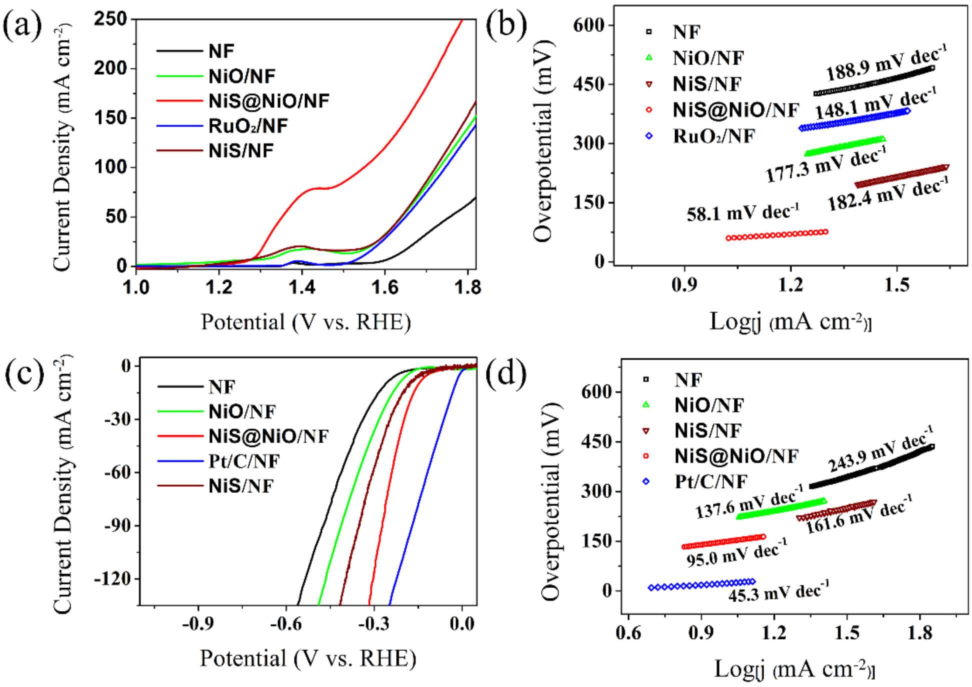

**Figure 4.** (a, b) OER and (c, d) HER performances for NiO/NF, NiS@NiO/NF, NiS/NF, bare NF, commercial Pt/C and $RuO_2$ in 1 M KOH. (a), (c) Polarisation curves of the samples at a scan rate of 5 mV $s^{-1}$. (b), (d) Corresponding Tafel plots derived from the polarisation curves.

The improvement in surface area, which results in the high catalyst performance, can be attributed to the observed structures. In **Fig. 3b,** a core structure with a spacing of 0.24 nm was represented by the (101) nanocrystalline plane belonging to the NiO phase; in the shell part, the crystal plane with a spacing of 0.20 nm can be defined to represent the (102) plane of NiS. This result is in agreement with the obtained XRD result, denoting the presence of a distinct heterogeneous interface structure between the NiS and NiO phases, which provide sufficient high-activity sites. It is well known that rich interface which cannot find in NiO/NF and NiS/NF can provide a large number of active sites for catalytic reactions, which will greatly facilitate OER and HER on the catalyst surface. Further, the NiS@NiO/NF sample exhibited a 3D layered porous structure with the NiO nanosheet core being wrapped by the NiS nanoflake shell.

A standard three-electrode electrochemical device was established in a 1.0 M KOH electrolyte to evaluate the bifunctional electrocatalytic activity of the prepared samples. First, the LSV polarisation curve was verified to determine the sample exhibiting the optimal vulcanisation degree. Based on the performances of the HER and OER, the sample treated using 0.8 g sulfur, represented as NiS@NiO/NF, was observed to exhibit the most outstanding catalytic performance. Also, the bare NF and commercial $RuO_2$ loading on the Ni foam ($RuO_2$/NF) were tested for comparison under identical conditions. As shown in the OER LSV curves of **Fig. 4a**, NiS@NiO/NF only requires an overpotential of 319 mV to achieve a large current density of 100 mA $cm^{-2}$, which is significantly less than those required by the bare Ni foam (706 mV), NiS/NF (492 mV) and NiO/NF (503 mV). This indicates that the nanointerfaces between NiS and NiO play an essential role in reducing the OER overpotentials. Furthermore, the presented OER performance of NiS@NiO/NF considerably exceeds that of the state-of-art $RuO_2$ (515 mV) and ranks one of the most active precious-metal-free electrocatalysts previously reported (as seen in Table 1) [31-35]. The fitted Tafel value of the NiS@NiO/NF catalyst is 58.1 mV $dec^{-1}$, which is less than those of NiO/NF (177.3 mV $dec^{-1}$), NiS/NF (182.4 mV $dec^{-1}$), $RuO_2$/NF (148.1 mV $dec^{-1}$) and bare NF (188.9 mV $dec^{-1}$), thereby exhibiting considerably favourable OER kinetics. To fabricate bifunctional electrocatalysts for water splitting, the HER activities of all the prepared samples and commercial Pt/C were evaluated (**Fig. 4c**). NiS@NiO/NF exhibited the optimal performance at a current density of 10 mA $cm^{-2}$ with an overpotential of 150 mV, which is considerably less than those of NF (263 mV), NiO/NF (217 mV) and NiS/NF (184 mV). This is superior to those of the transition-metal-based nanocatalysts reported in literature (as seen in Table 2) [31-35]. The Tafel slope of NiS@NiO/NF for the HER is 95.0 mV $dec^{-1}$ (**Fig. 4d**), which is considerably less than those of NiO/NF (137.6 mV $dec^{-1}$), NiS /NF (161.6 mV $dec^{-1}$) and NF (243.9 mV $dec^{-1}$). This denotes that the NiS@NiO coupling heterointerfaces are beneficial for the enhanced HER reaction kinetics corresponding to the Volmer–Heyrovsky mechanism.

**Table 1.** Comparison of OER performances in alkaline solution of NiS@NiO/NF with previously reported OER electrocatalysts grown on Ni foam..

| **Catalyst** | ***Current density (mA $cm^{-2}$)*** | ***Overpotential (mV)*** | ***References*** |
|---|---|---|---|
| **NiS@NiO/NF** | 100 | 319 | This work |
| **Ni–Co–S/NF** | 100 | >450 | [31] |
| **$CoSe_2$/NF** | 100 | 340 | [32] |
| **$Co_3O_4$@$Ni_3S_2$/NF** | 100 | >450 | [33] |
| **$Ni_3S_2$/$Co_9S_8$** | 100 | 340 | [34] |

**Table 2.** Comparison of HER performances in alkaline solution of NiS@NiO/NF with previously reported HER electrocatalysts grown on Ni foam..

| Catalyst | *Current density (mA cm$^{-2}$)* | *Overpotential (mV)* | *References* |
|---|---|---|---|
| NiS@NiO/NF | 10 | 150 | This work |
| Ni–Co–P/NF | 10 | 156 | [31] |
| $Co_{1-x}Fe_x$-LDH/NF | 10 | 183 | [35] |
| $NiCoS_{0.14}O_{3.25}$ NSs/NF | 10 | 170 | [33] |

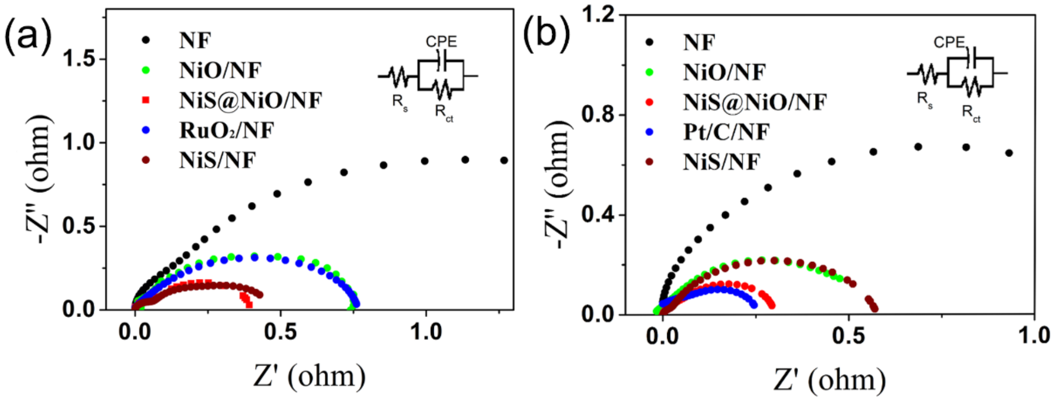

**Figure 5.** The EIS Nyquist plots for (a) the OER at a potential of 1.62 V vs. RHE and (b) the HER at a potential of −0.43 V vs. RHE for NiO/NF, NiS/NF, NiS@NiO/NF, bare NF, Pt/C/NF and $RuO_2$/NF. The insets in (a) and (b) denote the simplified equivalent circuits, where $R_s$ is the electrolyte resistance, $R_{ct}$ is the charge transfer resistance and CPE is the double layer capacitance.

The reaction resistance was studied via EIS to explore the high HER and OER activities of NiS@NiO/NF. **Figs. 5a** and **5b** denote the Nyquist plots of the prepared samples for OER and HER, respectively. Specific values of electrolyte resistance ($R_s$) and charge transfer resistance ($R_{ct}$) with respect to the HER and OER of all the samples in this study are presented in Tables S1 and S2. The results denote that the electronic transmission rate of NiS@NiO/NF is significantly higher than that of NiO/NF for both OER and HER, which can be mainly attributed to the fact that several NiS flakes exhibit excellent electrical conductivity. Consequently, the poor conductivity of NiO/NF is considerably improved. In case of OER, the charge transfer resistance ($R_{ct}$) of NiS@NiO/NF is less than that of the precious metal catalysts $RuO_2$/NF, whereas in case of HER, the $R_{ct}$ of NiS@NiO/NF is considerably similar to that of the noble metal catalysts Pt/C/NF. Furthermore, the electrochemical impedance of the NiS@NiO/NF catalyst with a poor-conductivity oxide substrate is less than that of the NiS/NF catalyst containing only a good-conductivity sulfide phase, revealing that this improvement in electrical conductivity can be attributed to the introducing interfaces [20, 21, 36-41].

The electrochemical active areas (ECSAs) of NiO/NF, NiS/NF and NiS@NiO/NF were determined by the electrical double layer capacitance ($C_{dl}$) method [42-45] based on the CV curves at different scanning rates (5, 10, 25, 50 and 100 mV s$^{-1}$) in the potential range from −0.05 to 0.05 V vs.

MOE (Fig. S3). As shown in **Fig. 6**, the corresponding $C_{dl}$ values for NiO/NF, NiS/NF and NiS@NiO/NF are 30.8, 36.4 and 78.6 mF cm$^{-2}$, respectively, demonstrating that the ECSA of NiS@NiO/NF is twice those of NiO/NF and NiS/NF, which can be attributed to the oxide/sulfide heterogeneous interface.

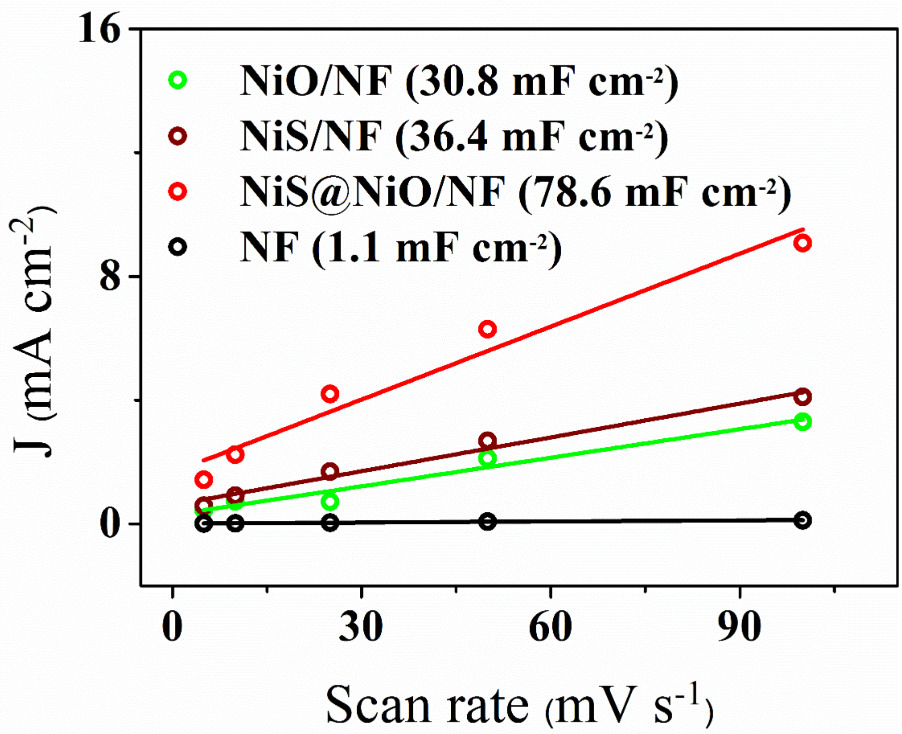

**Figure 6.** The ECSA values determined by the electrical double layer capacitance ($C_{dl}$) method for NiO/NF, NiS/NF, NiS@NiO/NF and NF.

Consequently, the increased geometrical/electrochemical active areas contribute to optimise the HER and OER performances. The remarkable OER and HER performances in case of NiS@NiO/NF can be attributed to the following factors: (i) the exposed interface and sulfides on the surface that considerably improve the electron transfer rate; (ii) the hierarchical porous structure that contribute to provide a considerable number of attachment points for the ions involved in the catalytic reaction and (iii) the exposed interface between the NiS and NiO phases provides considerably optimised active sites for the catalytic reaction.

The NiS@NiO/NF catalyst was used as the cathode and anode (designated as NiS@NiO/NF–NiS@NiO/NF) in 1.0 M KOH to evaluate the bifunctional overall water-splitting performance of the prepared catalyst. The overall water-splitting polarisation curves for several samples are presented in **Fig. 7**. The NiS@NiO/NF–NiS@NiO/NF system reveals an excellent overall water-splitting performance with an extremely low cell voltage of 1.54 V in the two-electrode system to achieve a current density of 10 mA cm$^{-2}$. This outstanding water-splitting performance is much better than the system consisting of precious metals catalysts Pt/C and $RuO_2$ (Pt/C - $RuO_2$/NF) (1.556 V), and superior to the Ni-based compounds grown on Ni foam reported recently in the literature (as seen in Table 3) [31,34, 46-48].

**Table 3.** Comparison of OER performances in alkaline solution of NiS@NiO/NF with previously reported water splitting electrocatalysts grown on Ni foam.

| Catalyst | *Current density ($mA\ cm^{-2}$)* | *Potential (V)* | *References* |
|---|---|---|---|
| NiS@NiO/NF | 10 | 1.54 | This work |
| Ni–Co–S// Ni–Co–P | 10 | 1.57 | [31] |
| Co–Ni–Se/C/NF | 10 | 1.60 | [46] |
| $Co_9S_8$-$Ni_3S_2$/NF | 10 | 1.59 | [34] |
| Co−Ni−S/NF | 10 | 1.60 | [47] |
| $Ni_3S_2/Co_9S_8$ | 10 | 1.55 | [48] |

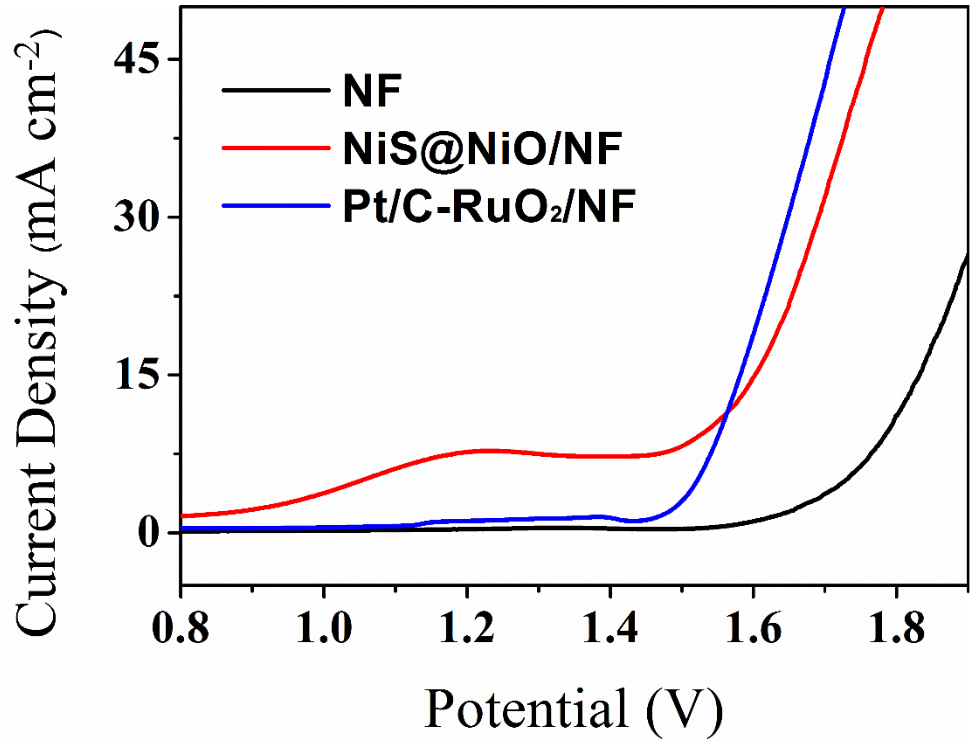

**Figure 7.** The overall water-splitting polarisation curves of NiS@NiO/NF, Pt/C - RuO2/NF and bare NF in 1.0 M KOH at a scan rate of 5 mV $s^{-1}$.

## 4. CONCLUSION

In this study, a hierarchical porous structure, comprising NiS nanoflakes supported on NiO nanosheets, was successfully synthesised on NF via a mild low-temperature hydrothermal sulfuration method. The core–shell NiS@NiO/NF array catalysts with a high specific surface area exhibit excellent bifunctional catalytic performances and remarkable long-term stability in an alkaline environment. The NiS@NiO/NF catalyst can be used with respect to the occurrence of HER at the cathode and OER at the anode in the overall water-splitting process. The cell voltage of the NiS@NiO/NF–NiS@NiO/NF system is as low as 1.54 V in 1.0 M KOH at a current density of 10 mA cm$^{-2}$. The excellent OER and HER performances of NiS@NiO/NF can be attributed to its good electrical conductivity, the extremely large specific surface area and the interfacial effect between two phases. Furthermore, its properties with respect to non-precious metals encourage its potential usage in large-scale industrial applications. This study also provides an efficient and rational method to grow self-assembled composite materials via ion exchange, which can be used as a reference for developing high-performance bifunctional materials in the future.

## SUPPLEMENTARY INFORMATION

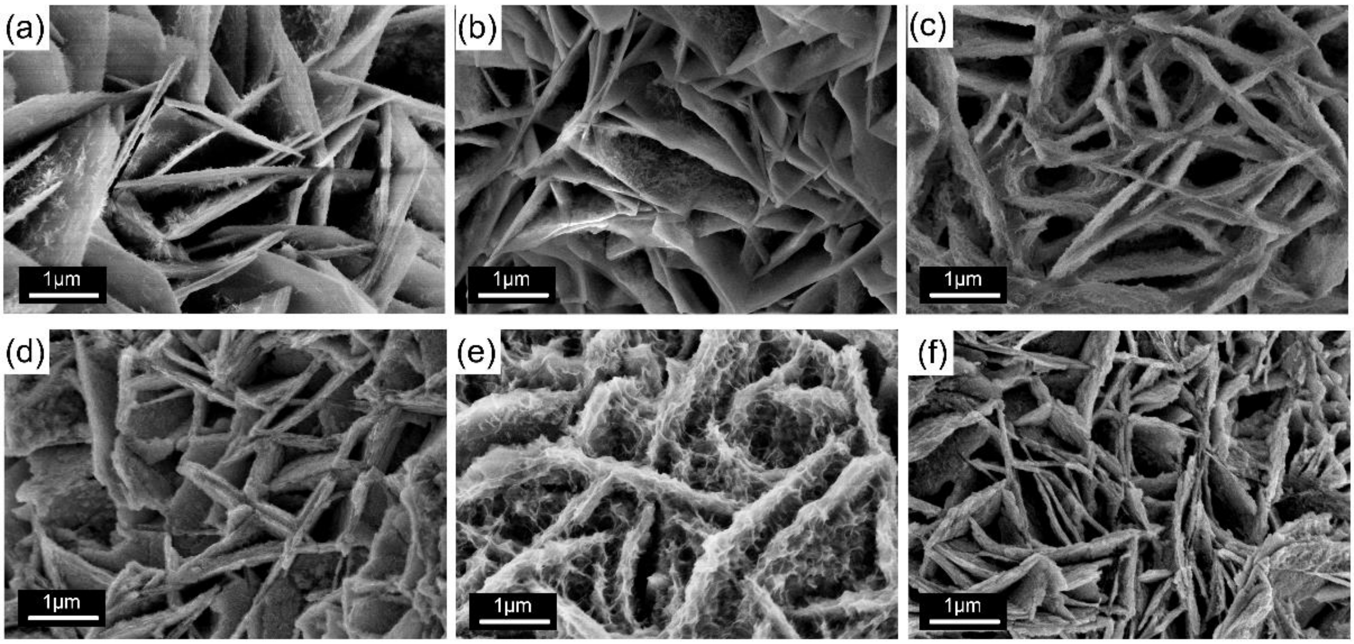

**Fig. S1.** SEM images of prepared NiS@NiO/NF samples with different $Na_2S$ amounts: (a) 0.2 g, (b) 0.4 g, (c) 0.6 g (d) 0.8 g, (e) 1.0 g and (f) 1.2 g.

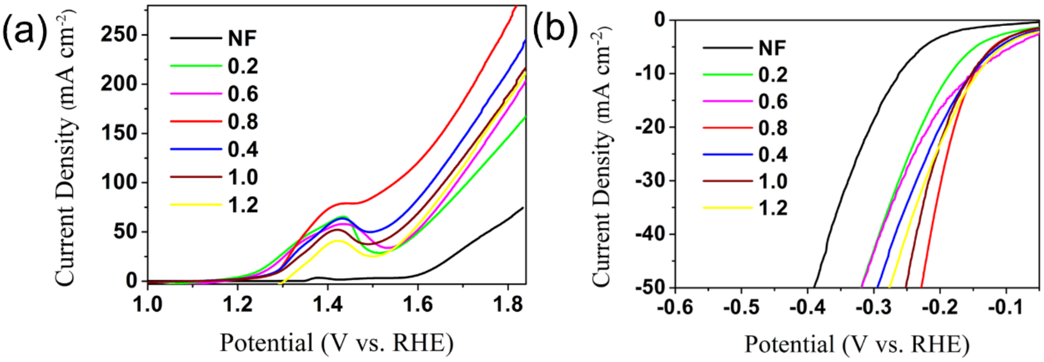

**Fig. S2.** (a) OER polarization curves and (b) HER polarization curves of different sulphide content samples of NiS@NiO supported on Ni foams.

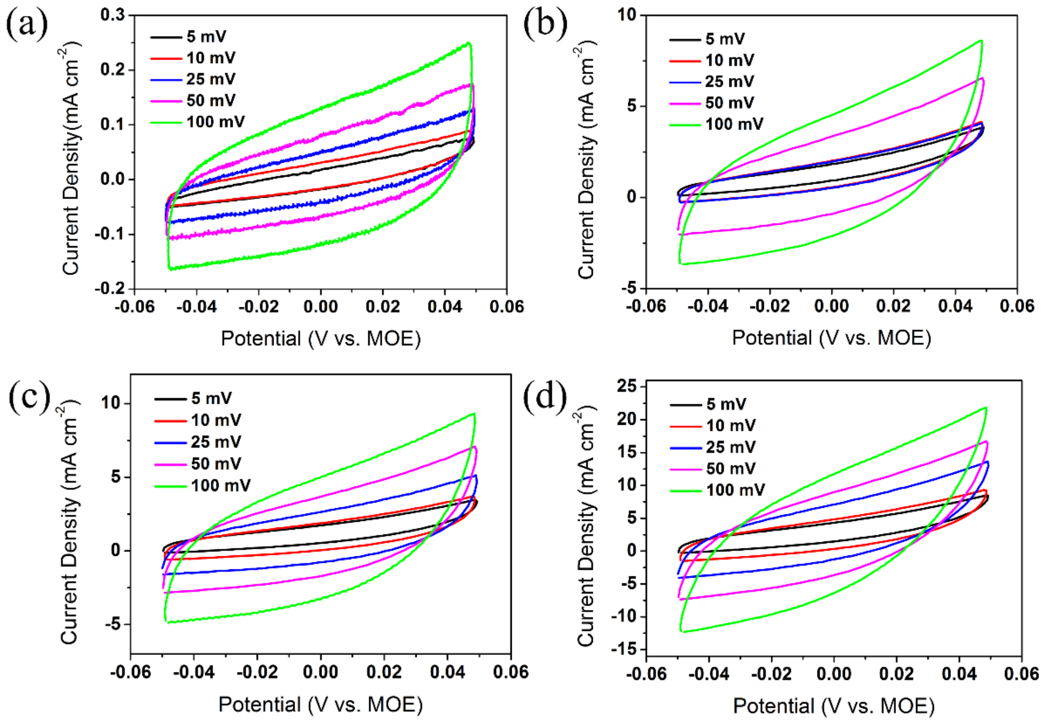

**Fig. S3.** CV curves of (a) NF, (b) NiO/NF, (c) NiS/NF and (d) NiS@NiO/NF at different scanning rates (5, 10, 25, 50, and 100 mV s$^{-1}$) in the potential range from -0.05V to 0.05 V vs. MOE.

**Table S1** Electrolyte resistances and charge transfer resistances toward OER in alkaline solution of all samples.

| **Sample** | $R_s$ (Ω) | $R_{ct}$ (Ω) |
|---|---|---|
| **NiS@NiO/NF** | 0.16 | 0.39 |
| **NiO/NF** | 0.32 | 0.74 |
| **NiS/NF** | 0.15 | 0.47 |
| **NF** | 0.90 | >2.6 |
| **RuO$_2$/NF** | 0.31 | 0.76 |

**Table S2** Electrolyte resistances and charge transfer resistances toward HER in alkaline solution of all samples.

| **Sample** | $R_s$ (Ω) | $R_{ct}$ (Ω) |
|---|---|---|
| **NiS@NiO/NF** | 0.12 | 0.3 |
| **NiO/NF** | 0.22 | 0.60 |
| **NiS/NF** | 0.22 | 0.57 |
| **NF** | 1.42 | 1.42 |
| **Pt/C/NF** | 0.10 | ~0.25 |

## References

1. N. T. Suen, S. F. Hung, Q. Quan, N. Zhang, Y. J. Xu and H. M. Chen, *Chem. Soc. Rev.*, 46(2017) 337.
2. C. Hu, L. Zhang and J. Gong, *Energy Environ. Sci.*, 12(2019) 2620.
3. S. H. Mohr, J. Wang, G. Ellem, J. Ward and D. Giurco, *Fuel*, 141(2015) 120.
4. M. Zhuang, G. L. Xu, L. Y. Gan, Y. Dou, C. J. Sun, X. Ou, Y. Xie, Z. Liu, Y. Cai, Y. Ding, I. H. Abidi, A. Tyagi, K. Amine and Z. Luo, *Nano Energy*, 58(2019) 660.
5. G. Zhou, Z. Guo, Y. Shan, S. Wu, J. Zhang, K. Yan, L. Liu, P. K. Chu and X. Wu, *Nano Energy*, 55(2019) 42.
6. D. Zhao, J. Dai, N. Zhou, N. Wang, P. Xinwen, Y. Qu and L. Li, *Carbon*, 142(2019) 196.
7. J. Zhang, M. Li, X. Liang and Z. Zhuang, *ACS Appl. Mater. Interfaces*, 11(2019) 1267.
8. Z. Zou, X. Wang, J. Huang, Z. Wu and F. Gao, *J. Mater. Chem. A*, 7(2019) 2233.
9. B. You, Y. Zhang, P. Yin, D. E. Jiang and Y. Sun, *Nano Energy*, 48(2018) 6000.
10. N. N. Han, K. R. Yang, Z. Y. Lu, Y. J. Li, W. W. Xu, T. F. Gao, Z. Cai, Y. Zhang, V. S. Batista, W. Liu and X. M. Sun, *Nat. Commun.*, 9(2018) 924.
11. P. W. Menezes, A. Indra, I. Zaharieva, C. Walter, S. Loos, S. Hoffmann, R. Schlögl, H. Dau and M. Driess, *Energy Environ. Sci.*, 12(2019) 988.
12. Z. Xiao, Y. Wang, Y. C. Huang, Z. Wei, C. L. Dong, J. Ma, S. Shen, Y. Li and S. Wang, *Energy Environ. Sci.*, 10(2047) 2563.
13. S. S. Yi, X. B. Zhang, B. R. Wulan, J. M. Yan and Q. Jiang, *Energy Environ. Sci.*, 11(2018) 3128.
14. H. Zhou, F. Yu, Q. Zhu, J. Sun, F. Qin, L. Yu, J. Bao, Y. Yu, S. Chen and Z. Ren, *Energy Environ. Sci.*, 11(2018) 2858.
15. X. Han, G. He, Y. He, J. Zhang, X. Zheng, L. Li, C. Zhong, W. Hu, Y. Deng and T.-Y. Ma, *Adv. Energy Mater.*, 8(2018) 1702222.
16. Y. He, J. Zhang, G. He, X. Han, X. Zheng, C. Zhong, W. Hu and Y. Deng, *Nanoscale*, 9(2017) 8623.
17. X. Han, X. Wu, Y. Deng, J. Liu, J. Lu, C. Zhong and W. Hu, *Adv. Energy Mater.*, 8(2018) 1800935.
18. X. Zheng, X. Wu, X. Han, Y. Deng and J. Wang, *Ferroelectrics*, 523(2018) 119.
19. X. C. Du, J. W. Huang, J. J. Zhang, Y. C. Yan, C. Y. Wu, Y. Hu, C. Y. Yan, T. Y. Lei, W. Chen, C. Fan and J. Xiong, *Angew. Chem. Int. Ed.*, 58(2019) 4484.
20. W. X. Zhu, C. Tang, D. N. Liu, J. L. Wang, A. M. Asiri and X. P. Sun, *J. Mater. Chem. A*, 4(2016) 7169.
21. H. C. Yang, Y. J. Zhang, F. Hu and Q. B. Wang, *Nano Lett*, 15(2015) 7616.
22. X. Zhao, J. Hu, S. Chen and Z. Chen, *PCCP*, 20(2018) 13637.
23. Q. H. Zhao, J. L. Yang, M. Q. Liu, R. Wang, G. X. Zhang, H. Wang, H. T. Tang, C. K. Liu, Z. W. Mei, H. B. Chen and F. Pan, *Acs Catalysis*, 8(2018) 5621.
24. Z. F. Zhang, Q. K. Qian, B. K. Li and K. J. Chen, *Acs Appl Mater Inter*, 10(2018) 17419.
25. Z. Zhang, X. X. Ma and J. L. Tang, *J. Mater. Chem. A*, 6(2018) 12361.
26. W. R. Zhang, D. H. Yan, X. Tong and M. Z. Liu, *Adv. Funct. Mater.*, 28(2018) 326.
27. T. T. Zhang, X. W. Liu, X. Cui, M. L. Chen, S. J. Liu and B. Y. Geng, *Advanced Materials Interfaces*, 5(2018) 443.
28. R. K. Zhang, F. Y. Ning, S. M. Xu, L. Zhou, M. F. Shao and M. Wei, *Electrochim. Acta*, 274(2018) 217.
29. M. D. Zhang, Q. B. Dai, H. G. Zheng, M. D. Chen and L. M. Dai, *Adv. Mater.*, 30(2018) 1800635.
30. M. Zhang, T. Li, J. Wang, Y. Pan, S. J. Ma, H. Zhu and M. L. Du, *Chinese J Inorg Chem*, 34(2018) 942.
31. J. Li, W. Xu, J. Luo, D. Zhou, D. Zhang, L. Wei, P. Xu and D. Yuan, *Nano-micro letters*, 10(2018)6.
32. D. Khalafallah, M. Zhi and Z. Hong, *Top Curr Chem (Cham)*, 377(2018) 29.

33. X. Zheng, X. Han, Y. Zhang, J. Wang, C. Zhong, Y. Deng and W. Hu, *Nanoscale*, 11(2018) 5646.
34. J. Li, P. Xu, R. Zhou, R. Li, L. Qiu, S. P. Jiang and D. Yuan, *Electrochim. Acta*, 299(2019) 152.
35. Y. Chen, K. Rui, J. Zhu, S. X. Dou and W. Sun, *Chemistry*, 25(2019) 703.
36. S. Sun, Z. Li, Z. A. Li, R. Xiao, M. Zhang, H. Tian, H. Yang and J. Li, *Nanoscale*, 10(2018) 7465.
37. E. Lee, E. Menumerov, R. A. Hughes, S. Neretina and T. Luo, *ACS Appl. Mater. Interfaces*, 10(2018) 34690.
38. Y. Zhang, J. Du, R. Luo, Z. Wang, Z. Wang, J. Han, P. Liu, T. Fujita, Q. Xue and M. Chen, *Nano Energy*, 58(2019) 552.
39. W. Q. Li, Y. H. Li, H. J. Wang, Y. H. Cao, H. Yu and F. Peng, *Electrochim. Acta*, 265(2018) 32.
40. Z. Zhang, Q. Wang, C. Zhao, S. Min and X. Qian, *ACS Appl. Mater. Interfaces*, 7(2015) 4861.
41. Q. Wang, X. Wang, B. Liu, G. Yu, X. Hou, D. Chen and G. Shen, *J. Mater. Chem. A*, 1(2013) 2468.
42. F. Zhang, Y. Ge, H. Chu, P. Dong, R. Baines, Y. Pei, M. Ye and J. Shen, *ACS Appl. Mater. Interfaces*, 10(2018) 7087.
43. G. Rajeshkhanna, T. I. Singh, N. H. Kim and J. H. Lee, *ACS Appl. Mater. Interfaces*, 10(2018) 42453.
44. J. Lin, H. Wang, X. Zheng, Y. Du, C. Zhao, J. Qi, J. Cao, W. Fei and J. Feng, *J. Power Sources*, 401(2018) 329.
45. C. Li, X. Zhao, Y. Liu, W. Wei and Y. Lin, *Electrochim. Acta*, 292(2018) 347.
46. Y. Gong, Z. Xu, H. Pan, Y. Lin, Z. Yang and J. Wang, *J. Mater. Chem. A*, 6(2018) 12506.
47. T. Yoon and K. S. Kim, *Adv. Funct. Mater.*, 26(2012) 7386.
48. F. Ming, H. Liang, H. Shi, X. Xu, G. Mei and Z. Wang, *J. Mater. Chem. A*, 4(2016) 15148.